Journal of Power Sources 195 (2010) 79–89

Contents lists available at ScienceDirect

Journal of Power Sources

journal homepage: www.elsevier.com/locate/jpowsour

Modelling and simulation of two-chamber microbial fuel cell

Yingzhi Zeng[a], Yeng Fung Choo[b], Byung-Hong Kim[b,c], Ping Wu[a,*]

[a] Institute of High Performance Computing, 1 Fusionopolis Way, #16-16 Connexis, Singapore 138632, Singapore
[b] Environment and Process Research Division, Korea Institute of Science and Technology, Hawolgok-dong, Sungbuk-ku, Seoul 136-791, Republic of Korea
[c] School of Life Science and Biotechnology, Korea University, Anam-dong, Sungbuk-ku, Seoul 136-701, Republic of Korea

ARTICLE INFO

Article history:
Received 5 March 2009
Received in revised form 10 June 2009
Accepted 24 June 2009
Available online 10 July 2009

Keywords:
Microbial fuel cell
Model
Parameter estimation
Simulation

ABSTRACT

Microbial fuel cells (MFCs) offer great promise for simultaneous treatment of wastewater and energy recovery. While past research has been based extensively on experimental studies, modelling and simulation remains scarce. A typical MFC shares many similarities with chemical fuel cells such as direct ascorbic acid fuel cells and direct methanol fuel cells. Therefore, an attempt is made to develop a MFC model similar to that for chemical fuel cells. By integrating biochemical reactions, Butler–Volmer expressions and mass/charge balances, a MFC model based on a two-chamber configuration is developed that simulates both steady and dynamic behaviour of a MFC, including voltage, power density, fuel concentration, and the influence of various parameters on power generation. Results show that the cathodic reaction is the most significant limiting factor of MFC performance. Periodic changes in the flow rate of fuel result in a boost of power output; this offers further insight into MFC behaviour. In addition to a MFC fuelled by acetate, the present method is also successfully extended to using artificial wastewater (solution of glucose and glutamic acid) as fuel. Since the proposed modelling method is easy to implement, it can serve as a framework for modelling other types of MFC and thereby will facilitate the development and scale-up of more efficient MFCs.

© 2009 Elsevier B.V. All rights reserved.

1. Introduction

A microbial fuel cell (MFC) is a device capable of directly transforming chemical energy into electrical energy via electrochemical reactions involving biochemical pathways. Unlike conventional fuel cells, which usually use precious metals as catalysts, MFCs use living organisms at mild conditions, namely, room temperature, atmospheric pressure, and neutral pH [1]. MFCs have operational and functional advantages over the technologies currently used for generating energy from organic matter [2]. One of the most active areas of MFC research in the past few years has been the production of power from organic waste [3]. While full scale and highly effective MFCs are not yet available, the technology holds great promise. The growing pressure for sustainable development and the call for renewable energy further motivate the development of this technology. Over the past years, considerable effort has been made to study the biological aspects such as the molecular analysis of the microbial community and electron transfer to electrodes in microorganisms [4,5], as well as developing various designs and configurations of MFCs [6,7]. Recent studies on the conversion of organic wastes to electricity have focused on the engineering challenges [3].

A number of limitations have hindered the wide implementation of MFCs. In particular, the power density of a MFC is several orders of magnitude lower than that of chemical fuel cells, and the technology is still only in the laboratory phase [8,9]. The extractable power from a particular fuel cell is restricted by a range of different parameters [2] that include the amount of bacterial cells, mixing and mass transfer phenomena in the reactors, bacterial kinetics, cathodic reactions, and the efficiency of the proton-exchange membrane. Therefore, construction and analysis of MFCs involve multidisciplinary knowledge of microbiology, electrochemistry, materials science, and engineering. Various intra-system phenomena and the effects of operating factors are not well understood. Investigating each parameter independently and/or all possible combinations of parameters using laboratory experiments is both costly and time consuming. Numerical modelling of a fuel cell system is a valuable tool for investigating system parameters with reduced time and money, as models can be easily modified to simulate various configurations and operating conditions. The development of a successful commercial MFC requires a 'chemical engineering' approach [10]. While modelling and simulation has been widely used to develop various chemical fuel cell systems, modelling and other forms of quantifications are often overlooked in MFC development [11]. Since the first MFC model was proposed

* Corresponding author. Tel.: +65 64191212.
E-mail addresses: zengyz@ihpc.a-star.edu.sg (Y. Zeng), pamcyf@gmail.com (Y.F. Choo), bhkim@kist.re.kr (B.-H. Kim), wuping@ihpc.a-star.edu.sg (P. Wu).

0378-7753/$ – see front matter © 2009 Elsevier B.V. All rights reserved.
doi:10.1016/j.jpowsour.2009.06.101

[12] to simulate a suspended cell with an added redox mediator, very little progress has been made in this field. Only very recently have computational models for biofilm-based microbial fuel cells been reported [13,14]. Since the models are comprehensive because of detailed descriptions of multi-species for the biofilm anode, modelling methods may not be readily implemented by the majority of the MFC community.

A typical two-chamber microbial fuel cell shares some similarities with chemical fuel cells such as direct methanol fuel cells (DMFCs) [15] and direct ascorbic acid fuel cells (DAAFCs) [16]. In both cases, anodic and cathodic chambers are separated by a cation-exchange membrane, fuels are oxidized in the anodic chamber and release protons that pass through the membrane to reach the cathodic chamber. Water saturated with oxygen is fed into the cathodic chamber, where the transported protons combine with dissolved oxygen. A MFC system is, however, remarkably different from chemical fuel cells in terms of the anodic reaction, fuel concentration, ion strength, pH, operating temperature, and purity of fuels. In particular, the fuel oxidation in a chemical fuel cell is often catalyzed by noble metals under high temperature, whereas a wide range of organic compounds can be catalyzed in a MFC by micro-organisms at room temperature. In addition, a variety of inorganic chemicals are employed to support the microbial metabolism in a MFC [5,17,18]. As a result, much more complicated bio-electrochemical reactions often take place in the anodic chamber of a MFC. Despite of the differences between chemical fuel cells and MFCs, we have been motivated by the successful development of mathematical models of a DMFC [15] and a DAAFC [16] that configurations similar to that of a typical two-chamber MFC. In the present study, these methodologies have been adopted to develop the MFC model by taking into account the bio-electrochemical reactions.

In the anodic compartment of a MFC, biological and electrochemical reactions take place via various mechanisms of electron transfer such as biofilm [14] and planktonic [19]. In this work, the model formulation is simplified with lump parameters of the fuel oxidation. Since the anodic chamber of a MFC operates at anaerobic or anoxic conditions, the biochemical kinetics are simulated in a similar fashion to that of a Anaerobic Digestion Model No. 1 (ADM1) [20]. As in the case of DAAFC, the rate of reaction is controlled by the electrical potential in an electrochemical cell and therefore the Butler–Volmer expression is incorporated. In comparison with chemical fuel cells, which use only pure fuel, MFCs often employ a variety of inorganic chemicals to support the microbial metabolism in addition to the fuel, which causes cations other than protons to dominate the mass transport via the proton-exchange membrane [5,17,18]. This issue is also addressed in the MFC modelling. As a first attempt, a mediator-less two-compartment MFC with a cation-exchange membrane was studied, and acetate was fed as the fuel since it is the most abundant fatty acid in anaerobic ecosystems and is used as an electron donor by anaerobic respiratory bacteria. The modelling method was extended to an artificial wastewater MFC fed with solution of glucose and glutamic acid.

The model is developed by integrating the bio-electrochemical kinetics and mass and charge balances within the MFC. Various parameters that significantly affect the MFC performance are investigated in the simulation, and the evolution in time of the MFC voltage, power density and fuel concentration are studied through dynamic simulation with stepped and periodic changes in the anodic feed flowrate. The developed method of MFC modelling is relatively simple and easy to implement, which may enhance its practical use in the design and operation of MFCs.

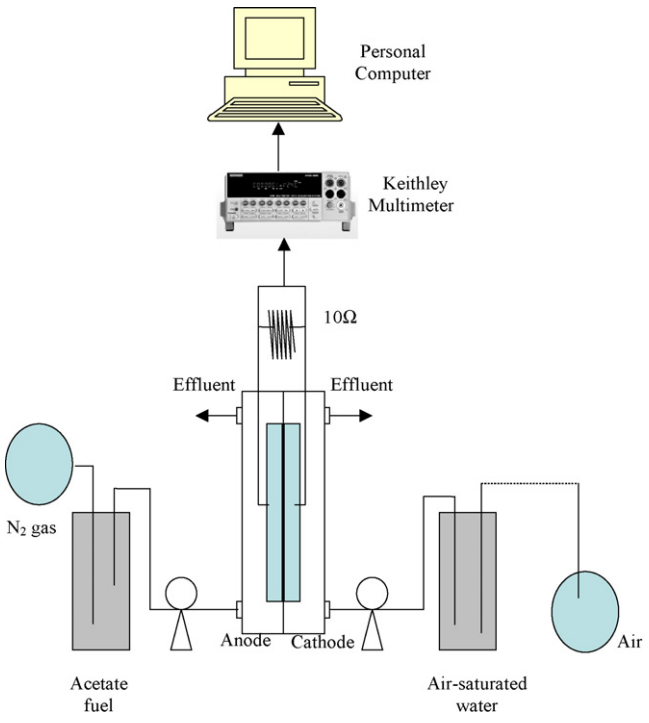

Fig. 1. Schematic diagram of acetate MFC experiment.

2. Methods of approach

2.1. Experiments

A schematic diagram of the experimental set-up is shown in Fig. 1. The working principle of the microbial fuel cell can be found elsewhere [21,22]. In the most general sense, microbial fuel cells function by oxidizing an electron donor with electron transfer at the anode under anoxic conditions. Electrons donated by the anode pass through a resistor or other type of electrical device to the cathode, which is submerged in aerobic water. In this work, the MFC device was made of transparent polyacrylic plastic. Each MFC consisted of anode and cathode compartments of equal volume (5.5 ml) and dimensions (5.5 × 1.0 × 1.0 cm). Each compartment contained two pieces (4.5 × 1.0 × 0.5 cm) of graphite felt (GF series, Electrosynthesis, Amherst, NY) as electrodes, but the graphite felt used for the cathode electrode was coated with 0.3 mg cm^{-2} of platinum powder [23]. The electrodes were connected via a platinum wire to a resistance box and a multimeter (Keithley Instruments, Cleveland, OH, USA). The anode and cathode chambers were separated by a cation-exchange membrane (Nafion®, Dupont Co., USA). Injection ports were installed in each chamber of the fuel cell. The anode chamber was kept anoxic by purging nitrogen gas. Throughout the study, the fuel containing 1.56 mM acetate and buffer solution (4 mM sodium acetate and inorganic salts) was continuously fed to the anode at the rate of 0.375 ml min^{-1}, and air-saturated tap water was fed into the cathode chamber as oxidant at the rate of 18.5 ml min^{-1}. Peristaltic pumps (505S, Watson-Marlow, Campel, UK) were used to feed the liquids that were pre-warmed to 30 °C. All experiments were conducted using three parallel microbial fuel cells installed in a temperature-controlled chamber at 30 °C and operated over one year. The external resistance between the anode and the cathode was systematically varied by means of a resistance box in the range of 10–10,000 Ω. The potential between the anode and the cathode was measured with the multimeter and recorded on a personal computer through a data-acquisition system (Testpoint, Capital Equipment, Richmond, VA, USA). The data was taken only when steady-state conditions had been established after changing the external resistance and took up to 30 min. The average or typical readings of the three fuel cells were used in model development and verification.

2.2. Model development

Experiments suggest that acetate is oxidized in the anode by the reaction of an eight-electron transfer as described in Eq. (R1). Since the anode chamber operates under anaerobic or anoxic conditions, the acetate degradation/oxidation can be modelled in a similar manner to ADM1, where a Monod-type equation is adopted. In addition, the operating conditions remain nearly unchanged except for variations in the external resistances. Various microbial consortia are thus lumped to a single quantity (biomass). Since (R1) is a bio-electrochemical reaction controlled by the electrical potential in an electrochemical cell, the Butler–Volmer expression is incorporated. Furthermore, since the reverse reaction is insignificant, only the forward reaction is used to formulate the reaction rate (Eq. (1)). It is noted that Eq. (1) is similar to the expression in the literature [14].

$$(CH_2O)_2 + 2H_2O \rightarrow 2CO_2 + 8H^+ + 8e^- \quad \text{(R1)}$$

$$r_1 = k_1^0 \exp\left(\frac{\alpha F}{RT}\eta_a\right) \frac{C_{Ac}}{K_{Ac} + C_{Ac}} X \quad (1)$$

where: C_{Ac} and X are the concentrations of acetate and biomass in the anode compartment, respectively; η_a is the anodic overpotential; k_1^0 is the rate constant of the anode reaction at standard conditions (maximum specific growth rate); K_{Ac} is the half velocity rate constant for acetate; α is the charge transfer coefficient of the anodic reaction, F is the Faraday constant, R is the gas constant, T is the cell operating temperature.

Since MFCs employ a variety of inorganic chemicals to support the microbial metabolism, cations such as K^+, Na^+, NH_4^+, Mg^{2+}, and Ca^{2+} are dissociated and their concentrations are typically 10^5 times higher than that of protons at neutral pH. Thus the number of cations transported from the anode to the cathode compartments other than protons are the same as the number of electrons transferred through the circuit [5,17,18]. This indicates that virtually no protons are transported in the MFC, and electro-neutrality is sustained mainly by the transport of cations instead of protons. An analysis [17] of a Nafion 117 membrane in a two-compartment MFC shows that K^+ and Na^+ occupied about 74% of the sulfonate residues. In order to maintain Nafion conductivity in the long run, the Nafion membrane was boiled in 0.1 M HCl before use to replace any cations attached to the sulfonate residues with protons. It is believed that the cation occupation is not permanent, but transient. Under these conditions, it is still possible for the cathode reaction to consume protons available from the dissociation of water.

For the sake of simplicity, it is assumed that only univalent cations M^+ transport through the membrane and the M^+ ions do not involve in the reaction at cathode. Consequently, the reduction of dissolved oxygen in the cathode is suggested as:

$$O_2 + 4e^- + 2H_2O \rightarrow 4OH^- \quad \text{(R2)}$$

It was found that dissolved oxygen exhibits Monod-type behaviour [5] and our preliminary study shows that the reverse reaction of oxygen reduction is negligible. Therefore, the rate of reaction in the cathodic chamber is formulated as Eq. (2). Again, the Butler–Volmer expression is incorporated to describe the electrochemical reaction.

$$r_2 = -k_2^0 \frac{C_{O_2}}{K_{O_2} + C_{O_2}} \exp\left[(\beta - 1)\frac{F}{RT}\eta_c\right] \quad (2)$$

where: C_{O_2} is the concentration of dissolved oxygen in the cathode compartment; η_c is the overpotential at the cathode; K_{O_2} is the half-velocity rate constant for dissolved oxygen; k_2^0 is the rate constant of the cathode reaction under standard conditions; β is the charge-transfer coefficient of the cathodic reaction. Water concentration is assumed constant (excess component in liquid mixture).

Similar to DAAFC modelling [16], it is assumed that both the anode and cathode compartments can be treated as a continuously stirred tank reactor (CSTR). Phase mixture, i.e., all mass-transport processes, is assumed to be so fast compared with the biochemical and redox reactions, such that the concentrations of all reactants in the bulk solution can be regarded to be equal to those on the surface of electrodes. In addition, carbon dioxide and acetate are assumed not to diffuse into the membrane, and the gas-phase formation by release of carbon dioxide bubbles is not taken into account. Consequently, the mass balances of the four components in the anode compartment, namely, acetate, dissolved CO_2, hydrogen ion and biomass, are expressed by Eqs. (3)–(6), respectively:

$$V_a \frac{dC_{Ac}}{dt} = Q_a(C_{Ac}^{in} - C_{Ac}) - A_m r_1 \quad (3)$$

$$V_a \frac{dC_{CO_2}}{dt} = Q_a(C_{CO_2}^{in} - C_{CO_2}) + 2A_m r_1 \quad (4)$$

$$V_a \frac{dC_H}{dt} = Q_a(C_H^{in} - C_H) + 8A_m r_1 \quad (5)$$

$$V_a \frac{dX}{dt} = Q_a \frac{(X^{in} - X)}{f_x} + A_m Y_{ac} r_1 - V_a K_{dec} X \quad (6)$$

In the above equations, the subscripts 'a' and 'in' denote the anode and the feed flow, respectively. V, Q and A_m are the volume of the compartment, the feed flow rate, and the cross-section area of membrane, respectively. In Eq. (6), f_x represents the reciprocal of the wash-out fraction, Y_{ac} the bacterial yield, and K_{dec} the decay constant for acetate utilisers.

In the cathode compartment, the mass balances of dissolved O_2, hydroxyl, and cation M^+ are expressed by Eqs. (7)–(9), respectively:

$$V_c \frac{dC_{O_2}}{dt} = Q_c(C_{O_2}^{in} - C_{O_2}) + r_2 A_m \quad (7)$$

$$V_c \frac{dC_{OH}}{dt} = Q_c(C_{OH}^{in} - C_{OH}) - 4r_2 A_m \quad (8)$$

$$V_c \frac{dC_M}{dt} = Q_c(C_M^{in} - C_M) + N_M A_m \quad (9)$$

The subscript 'c' denotes the cathode. In Eq. (9), N_M is the flux of M^+ ions transported from the anode to cathode compartment via the membrane. It is noted that the following relationship is held for the cell current density and the flux of ions via the membrane [24]:

$$i_{cell} = F\sum_i z_i N_i \quad (10)$$

where: z_i is the charge number of the ith species; N_i is the superficial flux of the ith species, i_{cell} denotes the cell current density. As mentioned previously, only M^+ ions are assumed to be transported through the membrane, thus the flux of M^+ ion (mol m^{-2} h^{-1}) can be calculated as follows, where the coefficient 3600 is the factor of unit conversion.

$$N_M = \frac{3600 i_{cell}}{F} \quad (11)$$

The charge balances at the anode and cathode are given by Eqs. (12) and (13), respectively, where C_a and C_c are the capacitances of the anode and cathode, respectively.

$$C_a \frac{d\eta_a}{dt} = 3600 i_{cell} - 8Fr_1 \quad (12)$$

$$C_c \frac{d\eta_c}{dt} = -3600 i_{cell} - 4Fr_2 \quad (13)$$

It is assumed that the ohmic drops in the current-collectors and electric connections are negligible, and the cell resistance is

Table 1
Parameters of experiment set-up and operation, and constants of acetate MFC model.

Symbol	Description	Unit	Value
F	Faraday's constant	Coulombs mol^{-1}	96485.4
R	Gas constant	J mol^{-1} K^{-1}	8.3144
T	Temperature	K	303
k^m	Electrical conductivity of membrane	Ohm^{-1} m^{-1}	17
d^m	Thickness of membrane	m	1.778×10^{-4}
k^{aq}	Electrical conductivity of the aqueous solution	Ohm^{-1} m^{-1}	5
d^{cell}	Distance between anode and cathode in the cell	m	2.2×10^{-2}
C_a	Capacitance of anode	F m^{-2}	4×10^{2}
C_c	Capacitance of cathode	F m^{-2}	5×10^{2}
V_a	Volume of anode compartment	m^3	5.5×10^{-5}
V_c	Volume of cathode compartment	m^3	5.5×10^{-5}
A_m	Area of membrane	m^2	5×10^{-4}
Y_{ac}	Bacterial yield	Dimensionless	0.05
K_{dec}	Decay constant for acetate utilisers	h^{-1}	8.33×10^{-4}
f_x	Reciprocal of wash-out fraction	Dimensionless	10
Q_a	Flow rate of fuel feed to anode	m^3 h^{-1}	2.25×10^{-5}
Q_c	Flow rate feeding to cathode compartment	m^3 h^{-1}	1.11×10^{-3}
C_{Ac}^{in}	Concentration of acetate in the influent of anode compartment	mol m^{-3}	1.56
$C_{CO_2}^{in}$	Concentration of CO_2 in the influent of anode compartment	mol m^{-3}	0
X^{in}	Concentration of bacteria in the influent of anode compartment	mol m^{-3}	0
C_H^{in}	Concentration of H^+ in the influent of anode compartment	mol m^{-3}	0
$C_{O_2}^{in}$	Concentration of dissolved O_2 in the influent of cathode compartment	mol m^{-3}	0.3125
C_M^{in}	Concentration of M^+ in the influent of cathode compartment	mol m^{-3}	0
C_{OH}^{in}	Concentration of OH^- in the influent of cathode compartment	mol m^{-3}	0
U^0	Cell open circuit potential	volt	0.77

solely due to the resistances of the membrane and the solution. Consequently, the cell voltage U_{cell} is calculated as:

$$U_{cell} = U^0 - \eta_a + \eta_c - \left(\frac{d^m}{k^m} + \frac{d_{cell}}{k^{aq}}\right) i_{cell} \quad (14)$$

where: U^0 is the open-circuit voltage; d^m and d_{cell} are the thickness of the membrane and the distance of the electrodes, respectively; k^m and k^{aq} are the conductivities of the membrane and the solution, respectively.

2.3. Parameter estimation

For the model system of Eqs. (1)–(14), the operating conditions, the parameters of the experimental set-up and the constants are listed in Table 1. Among them, the electrical conductivity of the aqueous solution (k^{aq}) is estimated, but it is not sensitive to simulation results. The parameters of the capacitances of the anode and cathode are not required for steady-state simulation and parameter estimation, but they are required to study the dynamic simulation. Similarly, although the two parameters are estimated from another study, they are not sensitive to the present results. Both bacterial yield and decay constant for acetate utilisers are taken from [25].

The six model parameters listed in Table 2 cannot be directly determined from experiments and thus are estimated by a mathematical method of best fitting of the experimental data. Specifically, the model parameters are estimated by minimizing the absolute differences between the measured and simulated cell voltages, namely, minimizing the quantity of F_{obj} defined in Eq. (15).

$$F_{obj} = \sum_{i=1}^{N} \left| U_i^{\exp} - U_i^{cal} \right| \quad (15)$$

where N is the number of data points, $U_i^{\exp}$ is the experimental measurements, and the simulated cell voltage U_i^{cal} is obtained from Eq. (14) by solving the model system of Eqs. (1)–(13) at the steady-state, namely, the algebraic equations obtained by setting all the derivatives to zeros.

3. Results and discussion

As mentioned early, three identical acetate MFC devices were used to conduct parallel experiments. During stable operation, the external resistance (R_{ex}) was varied and then fixed at 17 points in the range of 10–10,000 Ω. For each resistance, the MFC was allowed to establish its steady-state, which took up to 30 min. The resulting cell voltages (U_{cell}) were recorded and the cell currents (I_{cell}) were calculated with $I_{cell} = U_{cell}/R_{ex}$. Each data point was obtained by taking the average readings of the three devices, and 17 data points in total were obtained. Among them, 10 data points were selected for

Table 2
Estimated parameters of acetate MFC.

Symbol	Description	Unit	Resultant values
k_1^0	Forward rate constant of anode reaction at standard condition (maximum specific growth rate)	mol m^{-2} h^{-1}	0.207
k_2^0	Forward rate constant of cathode reaction at standard condition	m^{12} mol^{-4} h^{-1}	3.288×10^{-5}
K_{Ac}	Half velocity rate constant for acetate	mol m^{-3}	0.592
K_{O_2}	Half velocity rate constant for dissolved oxygen	mol m^{-3}	0.004
α	Charge transfer coefficient of anode	Dimensionless	0.051
β	Charge transfer coefficient of cathode	Dimensionless	0.663

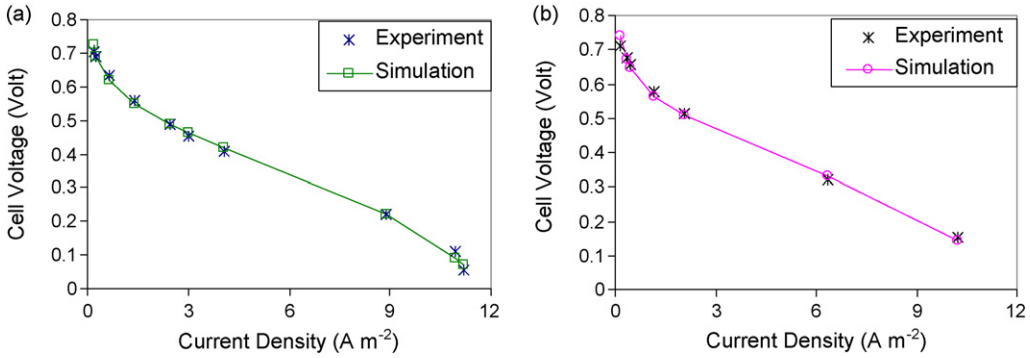

Fig. 2. Results from fitting experimental data (a) and model validation (b) for acetate MFC.

Table 3
Percentage changes in power density of acetate MFC when each parameter value is varied one at a time.

Ratio	k_1^0	k_2^0	K_{Ac}	K_{O_2}	α	β	Q_a	Q_c	C_{Ac}^{in}	$C_{O_2}^{in}$	d^{cell}	d^m	k^{aq}
0.8	−43.00	−6.55	18.37	0.08	10.23	63.01	−10.57	−0.01	−78.42	−0.12	1.86	0.01	−2.32
1.2	35.13	5.35	−16.71	−0.08	−6.82	−144.71	−17.47	0.01	31.09	0.08	−1.86	−0.01	1.55

parameter estimation by best fitting the model, and the remaining 7 data were used for model validation.

3.1. Resultant parameters and sensitivity analysis

As shown in Fig. 2a, good agreement is observed between the calculated and the measured cell voltages for a fitting set with the use of the 6 resultant model parameters. The average absolute difference is 0.01 V. The model is further examined by a validation set. Again, good agreement is found as shown in Fig. 2b where the average absolute difference is 0.01 V.

A preliminary sensitivity analysis on the operating, design and model parameters was investigated by varying each parameter, one at a time, while leaving the other parameters unchanged. Specifically, each parameter is varied by multiplying the 'ratio' to its original value at the base case—the experimental condition. The resultant average percentage changes in the power output over the range of cell current density (1–11.5 A m^{-2}) are listed in Table 3. As shown in the Table, when the parameter is reduced by a factor of 0.8, the acetate feed concentration leads to the largest decrease in power density over the entire range of cell current density, i.e., there is an absolute change of 78%. The next largest change is the electron transfer coefficient of the cathode (β), which leads to a boost of 63%. On the other hand, when the parameter is increased by a factor of 1.2, the cathode electron transfer coefficient results in the largest change, i.e., a decrease of 114%. The second and the third largest changes are caused by the rate constant of the anode reaction (35%) and the acetate feed concentration (31%). In both cases, the changes in the electrical conductivity of the aqueous solution k^{aq} is very small, namely, about 2%, which implies that it is insignificant to the accuracy of model prediction. It is also noted that the impacts of both cathode feed flowrate and dissolved oxygen concentration are very insignificant, and membrane thickness is the least sensitive.

The sensitivity of the 6 model parameters is further studied by the local relative sensitivity analysis method [26], to evaluate the ratio of changes in the computed power density to the changes in the parameters. The following equation is used for the 6 model parameters.

$$T_j = \frac{P(t, x_j + \delta x_j) - P(t, x_j)}{\delta x_j} \times \frac{x_j}{P(t, x_j)}, \quad j = 1, \ldots, 6 \tag{16}$$

where: T_j is time-dependent sensitivity of the jth parameters; x_j is the value of jth parameter; δx_j is the change in x_j; and P is the power density. In the present study, $\delta x_j = 0.01 x_j$. A dynamic simulation of step change in acetate feed flowrate from 2.2×10^{-5} to 1×10^{-5} ($m^3\,h^{-1}$) was conducted to examine the sensitivities of the 6 parameters. The results are shown in Fig. 3, and the order of parameter sensitivity (from the highest to the lowest) is $\beta > k_1^0 > \alpha > K_{Ac} > k_2^0 > K_{O_2}$. Apparently, the electron transfer coefficient β is the most sensitive parameter, whereas K_{O_2} is the least significant and remains almost unchanged.

The parameter sensitivity analysis has shown that the cathodic reaction may be the most significant factor limiting the performance of MFCs. This result agrees with the findings of Zhao et al. [18], who reported that the cathodic reaction often limits the performance of chemical fuel cells, such as polymer electrolyte membrane fuel cells and solid oxide fuels, and MFCs also share this problem. To improve the cathodic reaction, one of the most important issues is to develop efficient cathode materials which is, however, beyond the scope of this study and should be the focus of further investigation.

3.2. Steady-state simulation

With the parameters listed in Table 2, the component concentrations and reaction rates are evaluated with respect to the changes

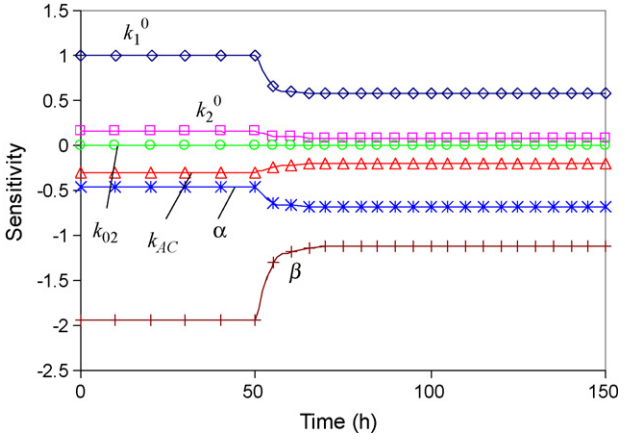

Fig. 3. Resultant sensitivities of 6 model parameters of acetate MFC model.

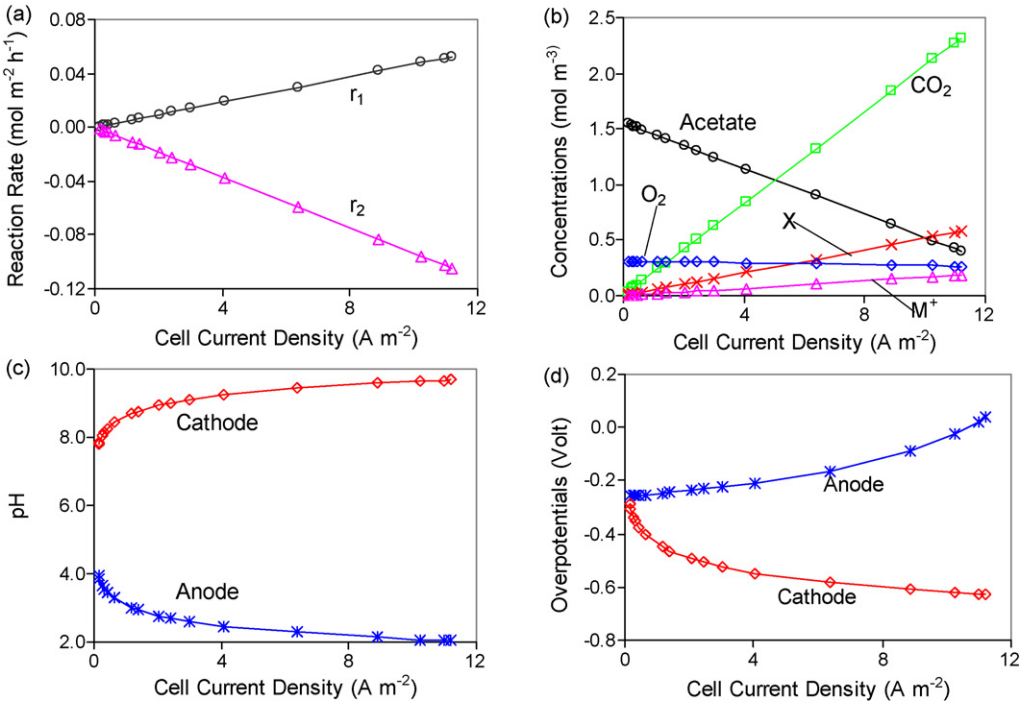

Fig. 4. Results of steady-state simulation of acetate MFC. (a) Reaction rates of acetate oxidation r_1 and oxygen reduction r_2; (b) concentrations of acetate, dissolved CO_2, biomass (X), dissolved oxygen (O_2) and M^+; (c) pH values in anode and cathode compartment; (d) overpotentials of anode and cathode.

in cell current density. As shown in Fig. 4a, the reaction rate of acetate oxidation in the anode chamber (r_1) and the rate of oxygen reduction ($-r_2$) in the cathode chamber are proportional to the cell current density. This behaviour can be explained by Eqs. (12) and (13) at the steady-state that are reduced to $r_1 = 450 i_{cell}/F$ and $r_2 = -900 i_{cell}/F$, respectively.

The resultant concentration of 5 components, i.e., acetate, CO_2, biomass (X) in the anodic chamber, and dissolved oxygen and M^+ in the cathodic chamber, are plotted in Fig. 4b. Obviously, CO_2 and biomass linearly increase while acetate decreases with respect to i_{cell}. Indeed, a higher current density leads to a faster reaction which consumes more fuel (acetate) and generates more CO_2. Similarly, a higher current density results in faster decrease in the dissolved oxygen in the cathode chamber although it is not pronounced. It follows from Eq. (9) that M^+ concentration is proportional to the M^+ flux, which is a linear function of cell current density (Eq. (11)). Therefore, M^+ concentration linearly increases with current density.

It can be seen in Fig. 4c that the pH in the anode compartment monotonically decreases as the cell current density increases, which indicates the anode compartment is acidified and the anode potential is raised (Fig. 4d). This result is in agreement with the experiment observations by other research groups [8,21]. By contrast, the pH in the cathodic compartment increases monotonously, which also agrees with the phenomena reported in [5].

As revealed from the parameter sensitivity analysis, the acetate flowrate (Q_a) and concentration (C_{Ac}^{in}) in the feed flow demonstrate the highest sensitivities among the operational and design parameters. The effects of the two parameters have therefore been further examined. Specifically, the two parameters have been varied by multiplying their original values by a factor of 0.8 and 1.2, respectively, while the other parameters remain unchanged. The simulation results are compared with that of the original experimental set-up (the Base Case). As shown in Fig. 5a, a decrease in acetate feed flowrate (Q_a) leads to a boost in power output until the cell current density is higher than 8.5 A m^{-2}. Beyond this point, an

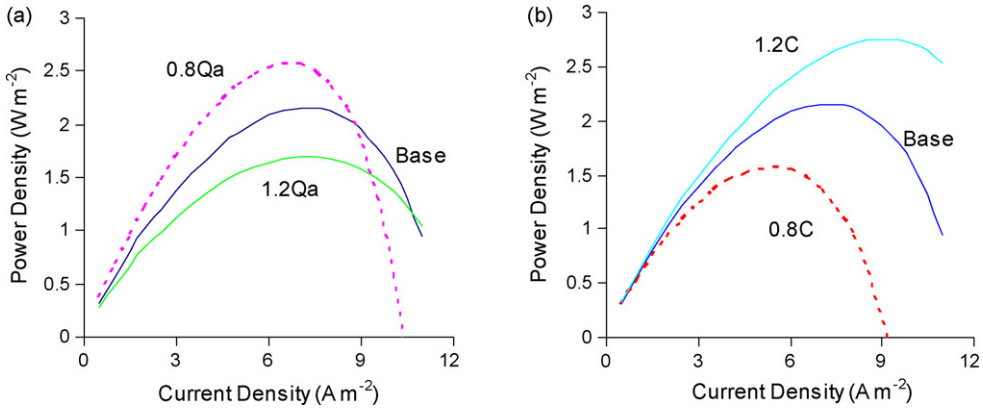

Fig. 5. Simulation results of variation in (a) acetate feed flowrate (Q_a); (b) acetate feed concentration (C). Q_a and C are varied by multiplying their original values by a factor of 0.8 and 1.2, respectively.

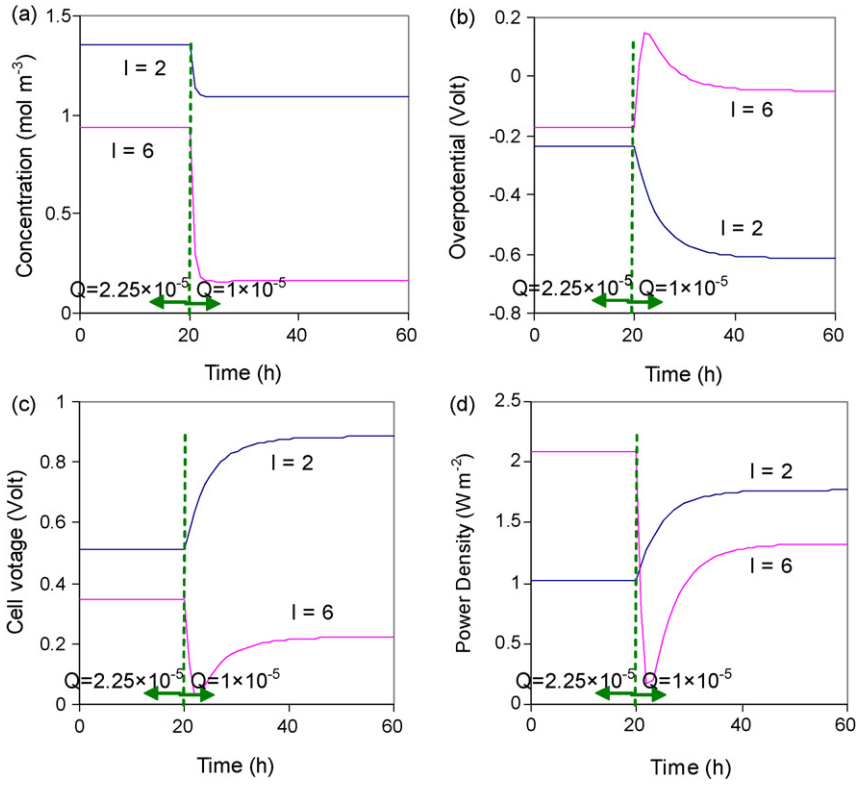

Fig. 6. Results of dynamical simulation of step change in acetate feed flowrate from 2.25×10^{-5} to 1×10^{-5} ($m^3\ h^{-1}$): (a) acetate concentration; (b) anode overpotential; (c) cell voltage; (d) power density.

extremely sharp decrease in power output is observed. An increase in Q_a demonstrates opposite behaviour. The result implies that a lower fuel feed flowrate may increase the power output but at the expense of a reduction in attainable current density. In order to maintain the same range of current density, the fuel concentration has to be increased. The effect of acetate feed concentration C_{Ac}^{in} is shown in Fig. 5b. An opposite effect to that of the feed flowrate is observed, i.e., cell current density is boosted by an increase in the feed concentration and the attainable current density also increases.

3.3. Dynamic simulation

In this study, the dynamic simulation of three scenarios has been performed, i.e., (1) a step decrease in acetate feed flowrate from 2.25×10^{-5} to 1×10^{-5} ($m^3\ h^{-1}$), (2) a step decrease in acetate feed concentration from 1.56 to 1 ($mol\ m^{-3}$), and (3) periodic changes in acetate feed flowrate from 2.25×10^{-5} to 1×10^{-5} ($m^3\ h^{-1}$). In each scenario, the cell current density is specified at 2 and 6 ($A\ m^{-2}$), respectively.

The result of the first scenario is shown in Fig. 6. The acetate concentration is reduced with a decrease in acetate feed flowrate (Fig. 6a) as explained by Eq. (17), and it is lowered even further if a higher cell current density is applied.

$$C_{Ac} = C_{Ac}^{in} - 450 i_{cell} \frac{A_m}{FQ_a} \tag{17}$$

The anode overpotentials exhibit opposite behaviour to the step decrease in acetate feed flowrate for different levels of cell current density (Fig. 6b). In particular, the anodic overpotential decreases when operating at lower current density, and vice versa. Since the cathodic overpotential is not affected by the change in acetate feed flowrate, the trends of cell voltage are opposite to those of the anode overpotentials (Fig. 6c). As a result, the power output increases when operating at lower current density and reduces at higher current density (Fig. 6d).

Dynamic simulation of the second scenario is shown in Fig. 7. Since a decrease in feed concentration enhances the anode overpotential (Eq. (18)) whereas the cathode overpotential is not affected by changes in acetate feed concentration, the cell voltage decreases as the feed concentration reduces. Furthermore, higher current density leads to an even larger anode overpotential, and thus a large drop in the cell voltage is observed (Fig. 7a). The resultant power density is the product of cell voltage and the cell current density (Fig. 7b).

$$\eta_a = \frac{RT}{\alpha F} \ln \left[\frac{Q_a + V_a K_{dec} f_x}{k_1^0 Y_{ac} A_m f_x} \left(\frac{K_{Ac}}{C_{Ac}^{in} - r_1 (A_m / Q_a)} + 1 \right) \right] \tag{18}$$

The result of the simulation for the third scenario is shown in Fig. 8 with the feed flowrate switching from 2.25×10^{-5} to $1 \times 10^{-5}\ m^3\ h^{-1}$ at equal intervals of 10 and 2 h, respectively. The resulting average power density of the two cases are 1.33 and 1.31 $W\ m^{-2}$ at a cell current density of $I = 2\ A\ m^{-2}$, and 2.14 and 2.11 $W\ m^{-2}$ at $I = 4\ A\ m^{-2}$, respectively. As can be seen, at $I = 2\ A\ m^{-2}$, the resulting average power density of periodic feeding is 1.32 $W\ m^{-2}$, which is higher than that of the steady-state, i.e., 1.01 $W\ m^{-2}$. Similarly, at $I = 4\ A\ m^{-2}$ periodic feeding results in 2.11 $W\ m^{-2}$, i.e., higher than that of the steady-state, 1.69 $W\ m^{-2}$. Furthermore, the choice of different intervals of flowrate switching does not lead to a significantly different average output, but smaller intervals tend to generate narrower variations which imply a more stable power output. The result indicates that feeding fuel in a periodic fashion may achieve a higher average power output.

3.4. Optimization

The optimum power output, subject to the existing MFC configuration and design, is studied in this section by manipulating the

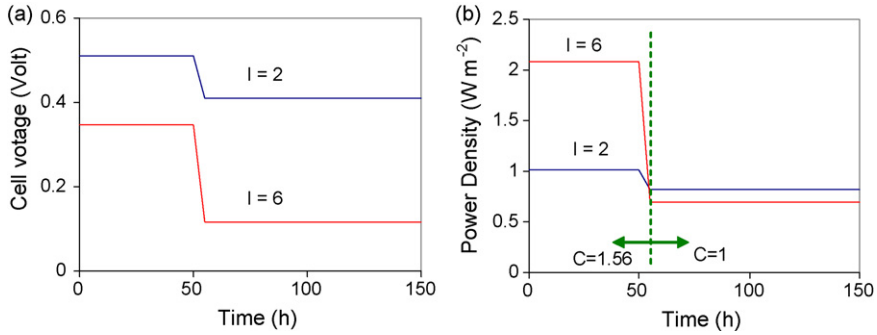

Fig. 7. Results of dynamical simulation of step change in acetate feed concentration from 1.56 to 1 (mol m^{-3}): (a) cell voltage; (b) power density.

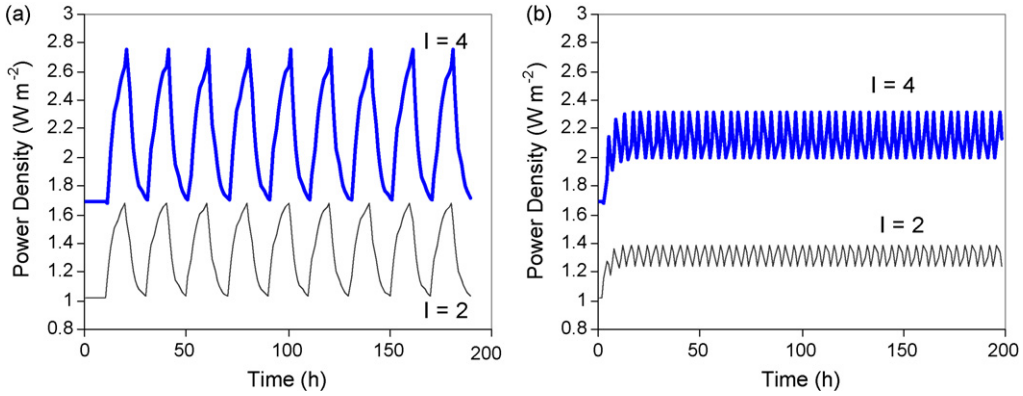

Fig. 8. Comparison of power outputs resulting from periodic switches of acetate feed flowrates from 2.25×10^{-5} to 1×10^{-5} m^3 h^{-1} with time intervals (a) $\Delta t = 10$ h, (b) $\Delta t = 2$ h. Cell current density is specified at $I = 4$ A m^{-2} and $I = 2$ A m^{-2} for each scenario, respectively.

Table 4
Comparison of maximum power output at optimum operating conditions and existing condition for acetate MFC.

Cases	Max. power density (W m^{-2})	Anode feed flowrate (m^3 h^{-1})	Cathode feed flowrate (m^3 h^{-1})	Current density (A m^{-2})
Experiment	2.0	2.2×10^{-5}	1.1×10^{-3}	8.9
Scenario #1	2.9	1.1×10^{-5}	1.3×10^{-3}	4.8
Scenario #2	2.4	2.0×10^{-5}	1.1×10^{-3}	7

flow rates of feed streams to the anode and cathode compartments. In Scenario #1, the current density is also allowed to vary so that a maximum power output is obtained at a particular current density. In Scenario #2, optimization is performed to search the maximum sum of power outputs over a set of equally spaced intervals of current densities within the range of the experiment. The results are presented in Table 4 and Fig. 9, and compared with the existing experiment. It is found that in Scenario #1, the highest power output 2.9 W m^{-2} is achieved at current density $I = 4.8$ A m^{-2}, but the optimum operating condition only sustains proper operation up to $I = 6.5$ A m^{-2}, which is much lower than the existing experiment viz., $I = 11.5$ A m^{-2}. In Scenario #2, the current density is no longer a manipulated variable for the optimization, thus the resulting operating condition (feed flow rates) is applicable to the entire range of the experiment. The resultant maximum power output is lower than that of Scenario #1, i.e., 2.4 W m^{-2} at $I = 7$ A m^{-2}, but still higher than that of the experiment maximum of 2.0 W m^{-2}. The result implies that the existing experiment has been operated at a sub-optimum condition, and reduction in the acetate feed flowrate may enhance the power output. Further decrease in the flowrate would reduce the attainable current density.

3.5. Simulation of GGA fuel cell

In this work, the modelling method is extended to a MFC fed by artificial wastewater, i.e., a solution of glucose and glutamic acid (GGA). The design configuration of the GGA MFC is similar to the acetate MFC described in the preceding sections. The experimental data reported in [27] is used for comparison with the simulated result.

The major difference between the GGA and acetate MFCs lies in the bio-electrochemical reactions occurring in the anodic chamber,

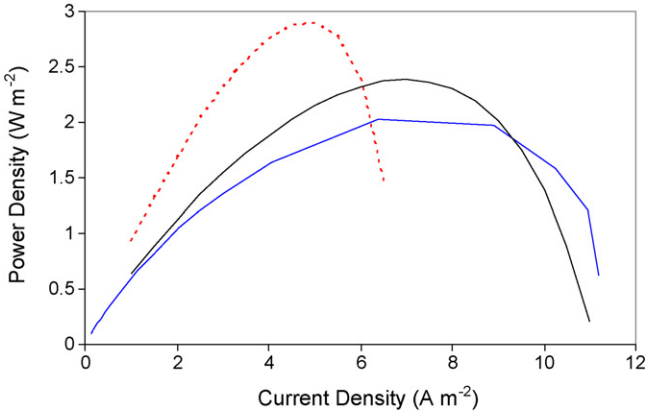

Fig. 9. Comparison of power densities among experimental measurements (bold line), by optimizing both feed flowrate and current density (dashed line), and by solely optimizing feed flowrate over entire range of current densities (fine line).

Table 5
Parameters of experiment set-up and operation of GGA MFC model.

Symbol	Description	Unit	Value
T	Operating temperature	K	306
V_a	Volume of anode compartment	m^3	2×10^{-5}
V_c	Volume of cathode compartment	m^3	2×10^{-5}
A_m	Area of membrane	m^2	2.4×10^{-3}
d^m	Thickness of membrane	m	5×10^{-3}
d^{cell}	Distance between anode and cathode in the cell	m	8.33×10^{-3}
Q_a	Flow rate of fuel feed to anode	$m^3\ h^{-1}$	2.1×10^{-5}
Q_c	Flow rate feeding to cathode compartment	$m^3\ h^{-1}$	5.7×10^{-4}
$C^{in}_{O_2}$	Concentration of dissolved O_2 in the influent of cathode compartment	$mol\ m^{-3}$	0.231
U^0	Cell open circuit potential	volt	0.75
k^0_2	Forward rate constant of cathode reaction at standard condition (from acetate MFC model)	$m^{12}\ mol^{-4}\ h^{-1}$	3.29×10^{-5}
K_{O_2}	Half velocity rate constant for dissolved oxygen	$mol\ m^{-3}$	4.06×10^{-3}

while the reduction reactions and mass balances in cathodic chamber of GGA MFC are the same as those of the acetate MFC. Since the feeding fuel is a mixture of glucose, glutamic acid and other inorganic compounds, the anodic reactions are taken as two oxidation reactions of glucose and glutamic acid, namely:

$$C_6H_{12}O_6 + 6H_2O \rightarrow 6CO_2 + 24H^+ + 24e^- \quad \text{(R11)}$$

$$C_5H_9NO_4 + 6H_2O \rightarrow 5CO_2 + NH^+{}_4 + 17H^+ + 18e^- \quad \text{(R12)}$$

The two reaction rates (Eqs. (19) and (20)) take a similar form as that of acetate MFC. k^{11}_0 and k^{12}_0 denote the rate constants of the corresponding reactions, C_6 and C_5 are the concentrations, and K_6 and K_5 are the half-velocity rate constants of glucose and glutamic acid, respectively. α_1 and α_2 designate the charge-transfer coefficients of the two reactions, respectively. It is noted that η_a (anode overpotential) and X (biomass concentration) are the same as those used in acetate MFC, but their values may be different in the GGA MFC.

$$r_{11} = k^0_{11} \exp\left(\frac{\alpha_1 F}{RT}\eta_a\right) \frac{C_6}{K_6 + C_6} X \quad (19)$$

$$r_{12} = k^0_{12} \exp\left(\frac{\alpha_2 F}{RT}\eta_a\right) \frac{C_5}{K_5 + C_5} X \quad (20)$$

The mass balances of five components in the anode chamber, i.e., concentrations of glucose, glutamic acid, dissolved CO_2, H^+ and biomass, are formulated similarly to those of the acetate MFC, namely:

$$V_a \frac{dC_6}{dt} = Q_a(C^{in}_6 - C_6) - A_m r_{11} \quad (21)$$

$$V_a \frac{dC_5}{dt} = Q_a(C^{in}_5 - C_5) - A_m r_{12} \quad (22)$$

$$V_a \frac{dC_{CO_2}}{dt} = Q_a(C^{in}_{CO_2} - C_{CO_2}) + 6A_m r_{11} + 5A_m r_{12} \quad (23)$$

$$V_a \frac{dC_H}{dt} = Q_a(C^{in}_H - C_H) + 24A_m r_{11} + 17A_m r_{12} \quad (24)$$

$$V_a \frac{dX}{dt} = \frac{Q_a(X^{in} - X)}{f_x} + A_m Y_{AW}(r_{11} + r_{12}) - V_a K_{dAW} X \quad (25)$$

Since the cathodic reaction in the GGA MFC is the same as that of acetate MFC, the rate expression, Eq. (2), remains unchanged in the model of the GGA MFC. Similarly, the mass balances in the cathode chamber, Eqs. (7)–(9), and the relationship of the cell current density and flux of ions via the membrane, Eq. (11), is used for the GGA MFC model.

The charge balance of the anode chamber is re-formulated in Eq. (26), while the charge balance of the cathode chamber and the cell voltage calculation remain unchanged as Eqs. (13) and (14), respectively.

$$C_a \frac{d\eta_a}{dt} = 3600 i_{cell} - 24 F r_1 \quad (26)$$

The experimental parameters that are different from the acetate MFC are listed in Table 5. Six data sets of experiments [27] with various combinations of artificial wastewater flowrates (Q_a) and concentrations (C_{AW}, in the unit of chemical oxygen demand, COD) are used in this study. The concentrations of glucose and glutamic acid in the influents are in the ratio of 1:1 in all the experiments. The range of Q_a ($ml\ min^{-1}$) is 0.15–0.65 and C_{AW} ($COD\ mg\ l^{-1}$) 100–300, respectively. In particular, the six sets of experiments are: (a) $C_{AW} = 100$, $Q_a = 0.35$; (b) $C_{AW} = 300$, $Q_a = 0.15$; (c) $C_{AW} = 200$, $Q_a = 0.65$; (d) $C_{AW} = 200$, $Q_a = 0.35$; (e) $C_{AW} = 300$, $Q_a = 0.35$; (f) $C_{AW} = 300$, $Q_a = 0.53$. The five model parameters (see Table 6) are estimated by using (a–d) sets of experimental data (see Fig. 10a–d), and the model is examined with (e and f) sets of experimental data (see Fig. 10e and f).

It is shown that all the simulation results generally reproduce the trends of the experimental results. On the other hand, relatively large deviations are observed when the wastewater concentration (C_{AW}) or flowrate (Q_a) is at the lower ends of the respective ranges in Fig. 10a ($C_{AW} = 100\ COD\ mg\ l^{-1}$) or Fig. 10b ($Q_a = 0.15\ ml\ min^{-1}$). The larger discrepancies may be caused by inconsistent experimental results [27], which showed that the I–V curves obtained from the two operation conditions significantly deviate from the others operated at higher C_{AW} or Q_a. The discrepancies may also arise from the fact that the model is unable to deal with an GGA MFC operating at extreme conditions, thus further improvement is required.

Table 6
Estimated parameters of GGA MFC.

Symbol	Description	Unit	Resultant values
k^0_{11}	Forward rate constant of glucose reaction at standard condition (maximum specific growth rate)	$mol\ m^{-2}\ h^{-1}$	5.94×10^{-1}
K_6	Half velocity rate constant for glucose	$mol\ m^{-3}$	3.68×10^{-5}
k^0_{12}	Forward rate constant of glutamic acid reaction at standard condition (maximum specific growth rate)	$mol\ m^{-2}\ h^{-1}$	7.35×10^{-3}
K_5	Half velocity rate constant for glutamic acid	$mol\ m^{-3}$	1.42×10^{-1}
α_1	Charge transfer coefficient of glucose oxidation at anode	Dimensionless	0.760
α_2	Charge transfer coefficient of glutamic acid oxidation at anode	Dimensionless	0.753
β	Charge transfer coefficient of cathode	Dimensionless	0.740

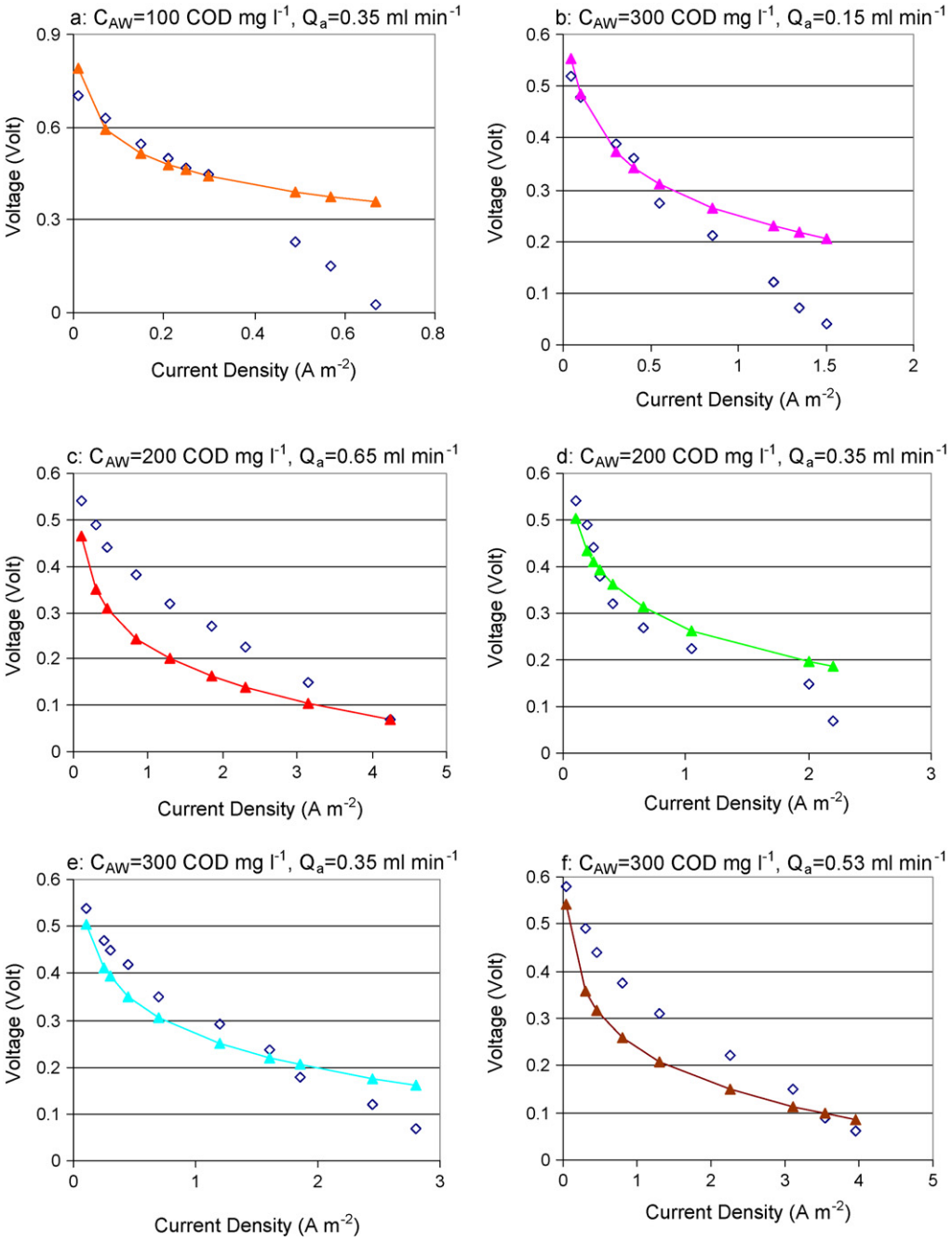

Fig. 10. Comparison of experimental (diamonds) and simulated (triangles) results for a GGA MFC, (a–d) fitting experiments; (e and f) model validation.

4. Conclusions

The present work describes a method for modelling the microbial fuel cell (MFC). The basis of the method is mass and charge balances with the integration of bio-electrochemical reactions. It is worthwhile to note that the model describes the experimental findings, i.e., virtually no protons are transported in the MFC and electro-neutrality is mainly sustained by the transport of cations instead of protons. The results of this modelling explain the trends in the experimental data under a steady or quasi-steady state, and give insights into how various parameters affect the power output. In particular, the cathodic reaction may be the most significant factor in limiting the performance of MFCs, which is in agreement with other published studies. Steady-state simulation demonstrates that a decrease in the fuel feed flowrate may lead to a boost in power output, but at the expense of reducing the attainable current density. Furthermore, the simulation also shows that an increase in fuel concentration is favorable in terms of power output and also allows the MFC to operate at a higher current density. The results of dynamic simulation suggest that a periodic change in fuel feed flowrate can yield higher average power output compared with steady state operation, which provides guidance for more efficient MFC designs and operational strategies.

While the model is developed based on an acetate MFC with a typical two-chamber design, the present study shows that the method can also be applied to a MFC fed with other fuels such as a solution of glucose and glutamic acid. It is noted that since the lump parameter method is used to formulate the model, some of the details, such as those occurring in the biofilm, cannot be predicted from the model. Nevertheless, models of MFCs with

various designs or operating conditions can be readily developed using this relatively simple method, which serves as a starting point for the development of more comprehensive MFC models that address more complicated issues relevant to MFC performance.

References

[1] B.H. Kim, H.J. Kim, M.S. Hyun, D.H. Park, J. Microbiol. Biotechnol. 9 (1999) 127–131.
[2] K. Rabaey, W. Verstraete, Trends Biotechnol. 23 (2005) 291–298.
[3] D.R. Lovley, Curr. Opin. Biotechnol. 17 (2006) 327–332.
[4] C.A. Pham, S.J. Jung, N.T. Phung, J.Y. Lee, I.S. Chang, B.H. Kim, H. Yi, J. Chun, FEMS Microbiol. Lett. 223 (2003) 129–134.
[5] B.E. Logan, C. Murano, K. Scott, N.D. Gray, I.M. Head, Water Res. 39 (2005) 942–952.
[6] H. Liu, B.E. Logan, Environ. Sci Technol. 38 (2004) 4040–4046.
[7] J.K. Jang, T.H. Pham, I.S. Chang, K.H. Kang, H.S. Moon, K.S. Cho, B.H. Kim, Process Biochem. 39 (2004) 1007–1012.
[8] L.T. Angenent, K. Karim, M.H. Al-Dahhan, R. Domiguez-Espinosa, Trends Biotechnol. 22 (2004) 477–485.
[9] B.H. Kim, I.S. Chang, G.M. Gadd, Appl. Microbiol. Biotechnol. 76 (2007) 485–494.
[10] R.A. Bullen, T.C. Arnot, J.B. Lakeman, F.C. Walsh, Biosens. Bioelectron. 21 (2006) 2015–2045.
[11] B.E. Rittmann, Trends Biotechnol. 24 (2006) 261–266.
[12] X.C. Zhang, A. Halme, Biotechnol. Lett. 17 (1995) 809–814.
[13] C. Picioreanu, I.M. Head, K.P. Katuri, M.C.M. van Loosdrecht, K. Scott, Water Res. 41 (2007) 2921–2940.
[14] A.K. Marcus, C.I. Torres, B.E. Rittmann, Biotechnol. Bioeng. 98 (2007) 1171–1182.
[15] S. Zhou, T. Schultz, M. Peglow, K. Sundmacher, Phys. Chem. Chem. Phys. 3 (2001) 347–355.
[16] Y. Zeng, N. Fujiwara, S.-i. Yamazaki, K. Tanimoto, P. Wu, J. Power Sources 185 (2008) 95–103.
[17] R.A. Rozendal, H.V.M. Hamelers, C.J.N. Buisman, Environ. Sci. Technol. 40 (2006) 5206–5211.
[18] F. Zhao, F. Harnisch, U. Schrorder, F. Scholz, P. Bogdanoff, I. Herrmann, Environ. Sci. Technol. 40 (2006) 5193–5199.
[19] M. Lanthier, K.B. Gregory, D.R. Lovley, FEMS Microbiol. Lett. 278 (2008) 29–35.
[20] D.J. Batstone, J. Keller, I. Angelidaki, S.V. Kalyuzhnyi, S.G. Pavlostathis, A. Rozzi, W.T.M. Sanders, H. Siegrist, V. Vavilin, Anaerobic Digestion Model No. 1 (ADM1), IWA Publishing, London, UK, 2002.
[21] G.C. Gil, I.S. Chang, B.H. Kim, M. Kim, J.K. Jang, H.S. Park, H.J. Kim, Biosens. Bioelectron. 18 (2003) 327–334.
[22] I.S. Chang, J.K. Jang, G.C. Gil, M. Kim, H.J. Kim, B.W. Cho, B.H. Kim, Biosens. Bioelectron. 19 (2004) 607–613.
[23] B.C. Jong, B.H. Kim, I.S. Chang, P.W.Y. Liew, Y.F. Choo, G.S. Kang, Environ. Sci. Technol. 40 (2006) 6449–6454.
[24] D.M. Bernardi, M.W. Verbrugge, AIChE J. 37 (1991) 1151–1163.
[25] ADM1 model for BSM2, International Water Association (IWA) Task Group on Benchmarking of Control Strategies for WWTPs, http://www.benchmarkwwtp.org/.
[26] A. Saltelli, K. Chan, E.M. Scott, Sensitivity Analysis, John Wiley and Sons, New York, 2000.
[27] H. Moon, I.S. Chang, B.H. Kim, Bioresour. Technol. 97 (2006) 621–627.